Geometrical Difference and Electron Configuration of Lantern-Type Rh_2^{4+} and Rh_2^{5+} Complexes: X-ray Structural and DFT Study

Takashi Kawamura,* Minobu Maeda, Makoto Miyamoto, Hiroshi Usami, Kaori Imaeda, and Masahiro Ebihara

Contribution from the Department of Chemistry, Faculty of Engineering, Gifu University, Yanagido, Gifu 501-1193 Japan

Received April 23, 1997. Revised Manuscript Received April 27, 1998

Abstract: Oxidation of $[Rh_2(O_2CEt)_4(PR_3)_2]$ (R: cy = cyclohexyl and Pr^i = iso-propyl) with ferrocenium ion gave stable salts of their cationic radicals. Their X-ray structures showed ca. 0.048 Å longer Rh−Rh and ca. 0.12 Å shorter Rh−P bonds than those of the diamagnetic neutral complexes. The pyramids of the phosphine ligands of these cationic complexes are more flattened than those of the neutral complexes. These observations and ESR data indicate that the σ_{RhRh} singly occupied molecular orbital (SOMO) of these complexes is extensively mixed with the phosphine lone-pair orbitals in the Rh−P σ antibonding phase. X-ray crystallographic structures of $[Rh_2(mhp)_4]^+$ (mhp = anion of 2-hydroxy-6-methylpyridine) and $[Rh_2(form)_4]^+$ (form = *N*,*N*′-di-*p*-tolylformamidinate anion) showed that the removal of a δ_{RhRh}* electron results in 0.017−0.043 Å decreases of their Rh−Eq bond distances, where Eq is the ligation atom in the bridging ligand. These results are consistent with the delocalization of the δ_{RhRh}* orbital (the SOMO of these cationic radicals) onto the bridging ligands in the π antibonding phase. B3LYP DFT calculations of Rh_2^{4+} and Rh_2^{5+} model complexes reproduced the ligand dependence of the electron configuration of Rh_2^{5+} complexes and geometrical changes accompanying the ionization and showed that the relatively rigid arrangement of the bridging ligands retards the dependence of the Rh−Rh bond length on the electron configuration. Also, the spin population in $[Rh_2(O_2CH)_4(PH_3)_2]^+$ is extensively delocalized onto the axial ligands, that in $[Rh_2(HNCHNH)_4]^+$ and $[Rh_2(HNCHO)_4(H_2O)_2]^+$ moderately onto the bridging ligands and that in $[Rh_2(O_2CH)_4(H_2O)_2]^+$ rather localized on the metal atoms.

Introduction

Since the assignment of the metal−metal quadruple bond to $[Re_2Cl_8]^{2-}$,[1] the electronic structure of metal−metal bonds in lantern-type M_2^{n+} complexes has been a subject of wide interest.[2,3] The electron configuration for the Rh−Rh bond in paramagnetic lantern-type Rh_2^{5+} complexes has been shown to depend on both axial and equatorial bridging ligands by analysis of ESR spin-Hamiltonian parameters.[4,5] The electron configuration of the Rh_2^{5+} complexes with π donative bridging ligands such as anions of amides, amidines, *o*-hydroxypyridines, or *o*-aminopyridines has been shown to be $\sigma^2\pi^4\delta^2\pi^{*4}\delta^{*1}$ (an example: $[Rh_2\{CH_3C(O)NH\}_4(NCCH_3)_2]^+$), that with strongly σ donating axial ligands such as phosphines and phosphites to be $\pi^4\delta^2\pi^{*4}\delta^{*2}\sigma^1$ (an example: $[Rh_2(O_2CEt)_4(PPh_3)_2]^+$), and that with weakly π donative bridges such as sulfate[5a] or carboxylates and weakly σ donating axial ligands such as O-ligands, nitriles and chloride ion to be $\sigma^2\pi^4\delta^2\delta^{*2}\pi^{*3}$ [5] (an example: $[Rh_2(OAc)_4(H_2O)_2]^+$). The electronic structure of Rh_2^{4+} and/or Rh_2^{5+} complexes has been calculated by using the SCCC,[6] extended Hückel,[7] ab initio Hartree−Fock,[8] Hartree−Fock followed by configuration interaction,[9] SCF Xα-SW,[10−12] and SCF Xα-DV methods.[13] Quite recently Cotton and co-workers[14] reported that the DFT calculations successfully reproduce structures and force constants of a variety of closed-shell lantern-type M_2^{2n+} complexes. Results of these calculations imply that the inclusion of correlation effects is essential for the calculation of the electronic structure of this class of complexes.[9]

Effects of an electron in Rh−Rh σ-, π-, and δ-type orbitals on the geometry have attracted attention to develop an understanding of the metal−metal bond. Zink and co-workers[15] estimated the structure of $[Rh_2(OAc)_4(YPh_3)_2]$ (Y = P, As, Sb) in the $\sigma_{RhRh}-\sigma_{RhRh}$* excited state on the basis of Raman spectroscopy. Geometrical changes resulting from one-electron oxidation of Rh_2^{4+} complexes to the corresponding Rh_2^{5+} with the configuration of $\sigma^2\pi^4\delta^2\pi^{*4}\delta^{*1}$ have been examined for some

(1) Cotton, F. A.; Harris, C. B. *Inorg. Chem.* **1965**, *4*, 330.
(2) Cotton, F. A.; Walton, R. A. *Multiple Bonds between Metal Atoms;* 2nd ed.; Oxford University Press: Oxford, 1993.
(3) (a) Cotton, F. A.; Ren, T. *Inorg. Chem.* **1995**, *34*, 3190. (b) Bear, J. L.; Han, B.; Huang, S.; Kadish, K. M. *Inorg. Chem.* **1996**, *35*, 3012.
(4) (a) Kawamura, T.; Fukamachi, K.; Hayashida, S. *J. Chem. Soc., Chem. Commun.* **1979**, 945. (b) Kawamura, T.; Fukamachi, K.; Sowa, T.; Hayashida, S.; Yonezawa, T. *J. Am. Chem. Soc.* **1981**, *103*, 364.
(5) (a) Baranovskii, I. B.; Zhilyaev, A. N.; Rotov, A. V. *Zh. Neorg. Khim.* **1985**, *30*, 3205. (b) Kawamura, T.; Katayama, H.; Yamabe, T. *Chem. Phys. Lett.* **1986**, *130*, 20. (c) Kawamura, T.; Katayama, H.; Nishikawa, H.; Yamabe, T. *J. Am. Chem. Soc.* **1989**, *111*, 8156.
(6) Dubicki, L.; Martin, R. L. *Inorg. Chem.* **1970**, *9*, 673.
(7) Rotov, A. V.; Ugolkova, E. A.; Rakin, Y. V. *Zh. Neorg. Khim.* **1991**, *36*, 1814.
(8) (a) Nakatsuji, H.; Ushio, J.; Kanda, K.; Onishi, Y.; Kawamura, T.; Yonezawa, T. *Chem. Phys. Lett.* **1981**, *79*, 299. (b) Nakatsuji, H.; Onishi, Y.; Ushio, J.; Yonezawa, T. *Inorg. Chem.* **1983**, *22*, 1623.
(9) (a) Mougenot, P.; Demuynck, J.; Benard, M. *Chem. Phys. Lett.* **1987**, *136*, 279. (b) Poblet, J. M.; Benard, M. *Inorg. Chem.* **1988**, *27*, 2935.
(10) (a) Norman, J. D., Jr.; Kolari, H. J. *J. Am. Chem. Soc.* **1978**, *100*, 791. (b) Norman, J. D., Jr.; Renzoni, G. E.; Case, D. A. *J. Am. Chem. Soc.* **1979**, *101*, 5256.
(11) Bursten, B. E.; Cotton, F. A. *Inorg. Chem.* **1981**, *20*, 3042.
(12) Cotton, F. A.; Feng, X. *Inorg. Chem.* **1989**, *28*, 1180.
(13) Rizzi, G. A.; Casarin, M.; Tondello, E.; Piraino, P.; Granozzi, G. *Inorg. Chem.* **1987**, *26*, 3406.
(14) Cotton, F. A.; Feng, X. *J. Am. Chem. Soc.* **1997**, *119*, 7514.
(15) Shin, K.-S.; Clark, R. J. H.; Zink, J. I. *J. Am. Chem. Soc.* **1989**, *111*, 4244.

S0002-7863(97)01294-8 CCC: $15.00
Published on Web 08/05/1998

examples.[16−18] The cationic radical salt of $[Rh_2(OAc)_4(H_2O)_2]ClO_4$[19] is the only example of the Rh_2^{5+} complex with the $\sigma^2\pi^4\delta^2\delta^{*2}\pi^{*3}$ configuration and with a reported X-ray structure. There is no report to our knowledge on the geometrical change induced by one-electron oxidation to the Rh_2^{5+} complex with the configuration of $\pi^4\delta^2\pi^{*4}\delta^{*2}\sigma^1$. Since the Rh−Rh σ orbital is important for the metal−metal bond and interesting from the viewpoint of σ-delocalization onto the axial ligands, we studied the X-ray structures of $[Rh_2(O_2CEt)_4(Pcy_3)_2]^+$ (**1**$^+$) and $[Rh_2(O_2CEt)_4(PPr^i_3)_2]^+$ (**2**$^+$), which are expected to have the $\pi^4\delta^2\pi^{*4}\delta^{*2}\sigma^1$ configuration,[4] and compared them with those of the closed-shell neutral mother complexes to see effects of a σ_{RhRh} electron on the geometry. We also report here X-ray structures of $[Rh_2(form)_4]^+$ (**3**$^+$, form = *N*,*N*′-di-*p*-tolylformamidinate anion) and $[Rh_2(mhp)_4]$ (**4**, mhp = anion of 2-hydroxy-6-methylpyridine) based on X-ray diffraction measured at low temperature. These and other experimentally observed geometrical changes are summarized and compared with density functional theory (DFT) calculations of model complexes with the hope of contributing to the development of a method to assign electronic structure from comparison of the geometry of a complex with its one-electron transferred one.

Experimental Section

Materials. Dirhodium complexes **1**,[20] **2**,[20] **3**,[21] and **4**[22] were prepared according to literature procedures. $FcSbF_6$, where Fc is ferrocene, was prepared by the reported method.[23] Silver perchlorate (Wako Chemicals) was dried under vacuum at room temperature for a few hours before use. Solvents (CH_2Cl_2, toluene, hexane, and CH_3CN) were distilled from P_2O_5 before use.

Apparatus. Cyclic voltammograms (CV) were observed by using BAS glassy carbon working and Pt wire counter electrodes; the redox potentials measured relative to a BAS RE−5 reference electrode (Ag^+/Ag/CH_3CN) were converted into those relative to the Fc^+/Fc potential as described previously.[24] UV-vis spectra were obtained on a Hitachi 3500 spectrophotometer at room temperature. IR spectra were recorded on a Perkin-Elmer 1600 FTIR spectrophotometer. ESR spectra were measured on a JEOL TE−200 spectrometer. Field sweep was monitored with an Echo Electronics EFM-2000 ^{1}H NMR gaussmeter, the probe of which was attached beside the ESR cavity; the field differences between the ESR and NMR sample positions were calibrated by measuring the field intensity at the resonance of perylene cationic radical in concentrated H_2SO_4 (g = 2.002583).[25] Elemental analyses were performed at the Elemental Analysis Center of Kyoto University.

$[Rh_2(O_2CEt)_4(Pcy_3)_2]SbF_6$ (5). To **1** (0.24 g, 0.23 mmol) in 20 mL of CH_2Cl_2, $FcSbF_6$ (0.098 g, 0.23 mmol) was added under argon and the solution was stirred for 1 h at room temperature. After evaporation of the solvent in vacuo, the black residue was washed with hexane and dissolved again into a small volume of CH_2Cl_2 followed by diffusion of hexane. The dark green microcrystalline solid contained CH_2Cl_2 as solvate molecules (vide infra) and disintegrated due to solvent loss at room temperature. The solid was placed under vacuum for 2 days to constant weight to give solvate-molecule free **5** (0.16 g, 0.12 mmol) in 52% yield. IR (KBr): 2932 (s), 2851 (m), 1575 (s), 1420 (s), 1301 (m), 1176 (m), 1111 (m), 1005 (m), 732 (m), 657 (s). UV−vis [CH_2Cl_2, λ_{max}/nm (log ϵ)]: 251 (3.84), 286 (sh), 428 (4.56), 518 (4.14). Anal. Calcd for $C_{48}H_{86}F_6O_8P_2Rh_2Sb$: C, 44.53; H, 6.70. Found: C, 44.34; H, 6.78.

$[Rh_2(O_2CEt)_4(PPr^i_3)_2]SbF_6$ (6). Complex **2** was oxidized by $FcSbF_6$ similarly as **1**. The cationic radical salt was recrystallized by slow diffusion of hexane into a concentrated CH_2Cl_2 solution of the salt as dark green microcrystals of **6** in 56% yield. IR (KBr): 2971 (m), 1578 (s), 1420 (s), 1303 (m), 1239 (m), 1061 (m), 862 (m), 658 (s). UV−vis [CH_2Cl_2, λ_{max}/nm (log ϵ)]: 251 (4.13), 285 (sh), 407 (4.15), 512 (3.72), 625 (sh). Anal. Calcd for $C_{30}H_{62}F_6O_8P_2Rh_2Sb$: C, 34.18; H, 5.93. Found: C, 34.46; H, 6.12.

$[Rh_2(form)_4]ClO_4$ (7). Since this perchlorate may be explosive, it should be handled with care in small quantities. To a solution of $[Rh_2(form)_4]\cdot 1.5C_6H_6$ (0.51 g, 0.42 mmol) in CH_2Cl_2 (50 mL) was added a toluene solution (20 mL) of $AgClO_4$ (94 mg, 0.45 mmol) and stirred for 1 h. After evaporation of the solvent to dryness, the residue was washed with toluene, extracted with CH_2Cl_2, and recrystallized by diffusion of toluene into the CH_2Cl_2 solution to give black microcrystals of **7** (0.36 g, 0.30 mmol) in 72% yield. Anal. Calcd for $C_{60}H_{60}ClN_8O_4Rh_2$: C, 60.13; H, 5.05; N, 9.35. Found: C, 59.95; H, 4.86; N, 9.31.

X-ray Crystallography. A prismatic orange-colored single crystal of **1** for X-ray crystallography was obtained by slow evaporation of its CH_2ClCH_2Cl solution. Slow evaporation of solvent from the CH_2ClCH_2Cl solution of **2** in a freezer gave its orange prismatic single crystal of X-ray quality. A yellow prismatic single crystal of **4**·CH_2Cl_2 was prepared by slow cooling of its CH_2Cl_2 solution in a freezer. X-ray diffraction data of **5**·$2CH_2Cl_2$ were collected for a prismatic dark green single-crystal grown by slow diffusion of *n*-hexane into a CH_2Cl_2 solution of this salt. The crystal lost solvate molecules at room temperature but was stable at temperatures below −30 °C. Layering of *n*-hexane on a CH_2Cl_2 solution of **6** gave its prismatic dark green single crystal. A prismatic greenish black single crystal of **7** was obtained by layering *n*-hexane on a CH_2Cl_2 solution of this salt.

The diffraction data were collected on a Rigaku AFC-7R diffractometer using graphite monochromated Mo Kα radiation (λ = 0.71069 Å). The crystals were placed on a glass fiber with silicone glue, mounted on a goniometer and cooled in cold nitrogen gas flow controlled by a Rigaku XR-TCS-2−050 temperature controller.

The positions of heavy atoms in the crystals of **1** and **2** were determined by direct methods (SHELXS-86).[26] The positions of all the non-H atoms of **4**·CH_2Cl_2 were refined starting from the room-temperature structure reported by Clegg and co-workers.[27] The lowering of the temperature of the diffraction collection from room temperature to the present −135 °C improved the deduced Rh−Rh bond length (decrease of the standard deviation from 0.001 to 0.0005 Å).

The structures of **5**·CH_2Cl_2, **6**, and **7** were solved with Patterson methods. In the crystal of **7**, the dirhodium unit lies on a 422 position. A difference Fourier map indicated disorder of the ClO_4^- ion around the other 422 site. Careful investigation of the map suggested not only the O atoms but also the Cl atoms were disordered. The Cl and O atoms were refined at fixed positions in tetrahedral arrangement with isotropic temperature factors.

X-ray absorption for crystals of **1**, **5**·$2CH_2Cl_2$, and **6** was corrected by using the ψ-scan method.[28] The ψ-scan absorption corrections for the crystals of **2**, **4**·CH_2Cl_2, and **7** did not improve analyses [$R(F_o)$, $R_w(F_o)$, and GOF] and were not applied. Calculations were performed by using the teXsan crystallographic software package provided by Molecular Structure Corp. Scattering factors for neutral atoms were

(16) Baranovskii, I. B.; Golubnichaya, M. A.; Dikareva, L. M.; Rotov, A. V.; Schelokov, R. N.; Porai-Koshits, M. A. *Zh. Neorg. Khim.* **1986**, *31*, 2876.
(17) Bear, J. L.; Yao, C.-Y.; Lofsey, R. S.; Korp, J. D.; Kadish, K. M. *Inorg. Chem.* **1991**, *30*, 336.
(18) Kawamura, T.; Ebihara, M.; Miyamoto, M. *Chem. Lett.* **1993**, 1509.
(19) Ziolkowski, J. J.; Moszner, M.; Glowiak, T. *J. Chem. Soc., Chem. Commun.* **1977**, 760.
(20) Sowa, T.; Kawamura, T.; Shida, T.; Yonezawa, T. *Inorg. Chem.* **1983**, *22*, 56.
(21) Piraino, P.; Bruno, G.; Schiavo, S. L.; Laschi, F.; Zanello, P. *Inorg. Chem.* **1987**, *26*, 2205.
(22) Berry, M.; Garner, C. D.; Hillier, I. H.; MacDowell, A. A.; Clegg, W. *J. Chem. Soc., Chem. Commun.* **1980**, 494.
(23) Sohn, Y. S.; Hendrikson, D. N.; Gray, H. B. *Inorg. Chem.* **1971**, *10*, 1559.
(24) Ebihara, M.; Tsuchiya, M.; Yamada, M.; Kawamura, T. *Inorg. Chim. Acta* **1995**, *231*, 35.
(25) Segal, B. G.; Kaplan, M.; Fraenkel, G. K. *J. Chem. Phys.* **1965**, *43*, 4191.
(26) Sheldrick, G. M. *SHELX86. Program for Crystal Structure Determination*; University of Göttingen: Göttingen, Germany, 1986.
(27) Clegg, W.; Garner, C. D.; Akhter, L.; Al-Samman, M. H. *Inorg. Chem.* **1983**, *22*, 2466.
(28) North, A. C. T.; Phillips, D. C.; Mathews, F. S. *Acta Crystallog.* **1968**, *A24*, 351.

Table 1. Crystallographic Data for $[Rh_2(O_2CEt)_4(Pcy_3)_2]$ (**1**), $[Rh_2(O_2CEt)_4(PPr^i_3)_2]$ (**2**), $[Rh_2(mhp)_4]\cdot CH_2Cl_2$ (**4**·CH_2Cl_2), $[Rh_2(O_2CEt)_4(Pcy_3)_2]SbF_6\cdot 2CH_2Cl_2$ (**5**·$2CH_2Cl_2$), $[Rh_2(O_2CEt)_4(PPr^i_3)_2]SbF_6$ (**6**), and $[Rh_2(form)_4]ClO_4$ (**7**)

compound	**1**	**2**	**4**·CH_2Cl_2	**5**·$2CH_2Cl_2$	**6**	**7**
chemical formula	$C_{48}H_{86}O_8P_2Rh_2$	$C_{30}H_{62}O_8P_2Rh_2$	$C_{25}H_{26}Cl_2N_4O_4Rh_2$	$C_{50}H_{90}Cl_4F_6O_8P_2Rh_2Sb$	$C_{30}H_{62}F_6O_8P_2Rh_2Sb$	$C_{60}H_{60}ClN_8O_4Rh_2$
formula weight	1058.96	818.57	723.22	1464.57	1054.31	1198.45
space group	$P2_1/n$ (14)	$P2_1/n$ (14)	$P2_1/n$ (14)	$P2_1/n$ (14)	$P\bar{1}$ (2)	$P4/nnc$ (126)
a/Å	14.879(1)	8.580(1)	12.647(2)	11.149(2)	12.442(2)	14.3327(8)
b/Å	9.6043(9)	12.820(2)	17.055(2)	18.902(3)	15.668(2)	14.3327(8)
c/Å	19.2032(9)	17.600(1)	12.663(2)	14.118(2)	11.598(2)	14.371(2)
α/deg	90	90	90	90	108.14(1)	90
β/deg	110.526(4)	101.012(8)	103.678(9)	94.45(1)	103.04(1)	90
γ/deg	90	90	90	90	94.85(1)	90
V/Å^3	2570.0(3)	1900.4(3)	2653.9(5)	2966.2(6)	2063.7(6)	2952.2(3)
Z	2	2	4	2	2	2
T/°C	−147	−62	−135	−147	−144	−20
ρ_{calc}/g cm^{-3}	1.368	1.430	1.810	1.640	1.697	1.348
crystal size/mm	0.20 × 0.29 × 0.43	0.10 × 0.20 × 0.44	0.10 × 0.15 × 0.25	0.25 × 0.25 × 0.28	0.16 × 0.20 × 0.35	0.25 × 0.30 × 0.30
μ(Mo Kα)/cm^{-1}	7.51	9.92	14.81	13.01	15.87	6.54
abs correction	ψ-scan	not applied	not applied	ψ-scan	ψ-scan	not applied
range of 2θ/deg	3−55	3−55	3−55	3−55	3−55	3−55
collected[a]	6501	4857	7260	7398	9906	3815
unique[b]	4110	3341	3585	5249	8080	932
variables[c]	443	310	334	511	666	84
$R(F_o)$[d]	0.025	0.031	0.033	0.025	0.025	0.037
$R_w(F_o)$[e]	0.029	0.028	0.041	0.027	0.029	0.046
p[e]	0.014	0.002	0.022	0.012	0.009	0.020
residual/e Å^{-3} [f]	−0.70, 0.68	−0.56, 0.73	−0.63, 0.89	−0.56, 0.41	−0.84, 0.57	−2.02, 1.84
GOF	1.456	1.489	1.177	1.301	1.682	1.744

[a] Number of collected reflections. [b] Number of unique reflections with $I > 3\sigma(I)$. [c] Number of variables in the final refinement. [d] $R = \sum||F_o| - |F_c||/\sum|F_o|$. [e] $R_w = [\sum w(|F_o| - |F_c|)^2/\sum w|F_o|^2]^{1/2}$, $w = 1/[\sigma^2(F_o) + (p^2/4)\,|F_o|^2]$. [f] Minimum and maximum residual peaks in the final difference Fourier map: min, max.

from Cromer and Waber[29] and anomalous dispersion[30] was included. Crystal data and details of refinements for the structure determination of **1**, **2**, **4**·CH_2Cl_2, **5**·$2CH_2Cl_2$, **6**, and **7** are listed in Table 1.

Calculation of Electronic Structure and Geometry Optimization. This was performed based on the restricted and unrestricted DFT method with the B3LYP functional[31] by using the Gaussian 94 program.[32] The effective core potentials and the basis functions for the Rh and P atoms were those of LANL2DZ (split valence type)[33] built in Gaussian 94. The basis set for the P atom was supplemented with a single primitive d-type polarization function of $\alpha = 0.34$.[34] The 6-31G split valence set[35] was used for the H, N, and O atoms. The d functions were of the mutually orthogonal five-function type. Geometry of $[Rh_2(O_2CH)_4(PH_3)_2]^{0/+}$ (**8**$^{0/+}$, C_{2v} with the C_2 axis perpendicular to the Rh−Rh bond), $[Rh_2(O_2CH)_4(H_2O)_2]^{0/+}$ (**9**$^{0/+}$, C_{2v} with the Rh−Rh bond as the C_2 axis), and $[Rh_2(HNCHNH)_4]^{0/+}$ (**10**$^{0/+}$, C_{2v} with the Rh−Rh bond as the C_2 axis) was optimized in the symmetry given in the parentheses to the default criteria of Gaussian 94. The geometry of *cis*-(2,2)-$[Rh_2(HNCHO)_4(H_2O)_2]^{0/+}$ (**11**$^{0/+}$, C_i) was optimized by freezing the Rh−O_{ax}-H_{ax} bond angles and one of O_{eq}-Rh−O_{ax}-H_{ax} dihedral angles for each of the axial ligands at the corresponding experimental values in the crystals of *cis*-(2,2)-$[Rh_2(HNCMeO)_4(H_2O)_2]$[36] and *cis*-(2,2)-$[Rh_2(HNCMeO)_4(H_2O)_2]ClO_4$[16] because in both of the crystals the axial H_2O ligands are involved in intermolecular hydrogen bonding. To examine the dependence of Rh−Rh, Rh−P, and Rh−O bond lengths on the O···O nonbonded separation in the bridging formato ligands in **8**, the geometry of the complex was optimized in the C_{2v} geometry with freezing the bridging formates at various geometries to artificially adjust the O···O separation by changing the O−C−O angles. To see the rigidness of the Rh−O_{ax} and Rh−O_{eq} bonds in **11**$^{0/+}$ and of the Rh−P bonds in **8**$^{0/+}$, their force constants were estimated by comparing total energies at optimized structures with their bond distances at artificially frozen various values. The natural bond orbital (NBO) method[37] built in Gaussian 94 was utilized for the analysis of electron population and hybridization.

Results and Discussion

Structure of $[Rh_2(O_2CEt)_4(Pcy_3)_2]$ (1), $[Rh_2(O_2CEt)_4(PPr^i_3)_2]$ (2), and $[Rh_2(mhp)_4]$ (4). ORTEP views and geometry parameters for **1** and **2** are reported in Supporting Information. The structure of **4** deduced from X-ray diffraction data collected at room temperature has been reported by Clegg and co-workers,[27] but it was reexamined at −135 °C to obtain more detailed structure parameters to be compared with those of its cationic radical salt at the same temperature in our previous report.[18] The atomic numbering scheme and structure parameters of this complex are also reported in Supporting Information.

CV and Oxidation of $[Rh_2(O_2CEt)_4(PR_3)_2]$ and ESR of $[Rh_2(O_2CEt)_4(PR_3)_2]^+$. Cyclic voltammograms of **1** and **2** in CH_2Cl_2 containing 0.1 mol/L of $Bu^n_4NClO_4$ as supporting electrolyte showed chemically reversible one-electron oxidation

(29) Cromer, D. T.; Waber, J. T. *International Tables for X-ray Crystallography*; The Kynoch Press: Birmingham, England, 1974; Vol. IV, Table 2.2 A.

(30) Creagh, D. C.; McAuley, W. J. *International Tables for Crystallography*; Wilson, A. J. C., Ed.; Kluwer Academic Publishers: Boston, MA, 1992; Vol. C, Table 4.2.6.8, pp 219−222.

(31) (a) Lee, C.; Yang, W.; Parr, R. G. *Phys. Rev.* **1988**, *B37*, 785. (b) Miehlich, B.; Savin, A.; Stoll, H.; Preuss, H. *Chem. Phys. Lett.* **1989**, *157*, 200. (c) Becke, A. D. *J. Chem. Phys.* **1993**, *98*, 5648.

(32) Frisch, M. J.; Trucks, G. W.; Schlegel, H. B.; Gill, P. M. W.; Johnson, B. G.; Robb, M. A.; Cheeseman, J. R.; Keith, T. A.; Petersson, G. A.; Montgomery, J. A.; Raghavachari, K.; Al-Laham, M. A.; Zakrewski, V. G.; Ortiz, J. V.; Foresman, J. B.; Cioslowski, J.; Stefanov, B. B.; Nanayakkara, A.; Challacombe, M.; Peng, C. Y.; Ayala, P. Y.; Chen, W.; Wong, M. W.; Andres, J. L.; Replogle, E. S.; Gomperts, R.; Martin, R. L.; Fox, D. J.; Binkley, J. S.; Defrees, D. J.; Baker, J.; Stewart, J. P.; Head-Gordon, M.; Gonzalez, C.; Pople, J. A. *Gaussian 94*; Gaussian, Inc.: Pittsburgh, PA, 1995.

(33) Hay, P. J.; Watt, W. R. *J. Chem. Phys.* **1985**, *82*, 270.

(34) Huzinaga, S.; Andzelm, J.; Klobukowski, M.; Radzio-Andzelm, E.; Sakai, Y.; Tatewaki, H. *Gaussian Basis Sets for Molecular Calculations*; Elsevier Science Pub.: Amsterdam, 1984.

(35) Ditchfield, R.; Hehre, W. J.; Pople, J. A. *J. Chem. Phys.* **1971**, *54*, 724.

(36) Ahsan, M. Q.; Bernal, I.; Bear, J. L. *Inorg. Chem.* **1986**, *25*, 260.

(37) (a) Glendening, E. D.; Reed, A. E.; Carpenter, J. E.; Weinhold F. *NBO Version 3.0 Program*; University of Wisconsin: Madison, WI, 1990. (b) Reed, A. E.; Curtiss, L. A.; Weinhold, F. *Chem. Rev.* **1988**, *88*, 899.

Table 2. ESR Parameters of $[Rh_2(O_2CEt)_4(PR_3)_2]SbF_6$ in CH_2Cl_2

PR_3	g(para)[a]	g(perp)[b]	A(para)[a,c]	A(perp)[b,c]	a[c,d]
Pcy_3	1.992	2.128	21.5	14.3	16.2
PPr^i_3	1.999	2.134	21.3	14.3	16.5

[a] Parallel component at 77 K. [b] Perpendicular component at 77 K. [c] Splitting due to two equivalent ^{31}P nuclei in unit of 10^{-3} cm^{-1}. [d] Isotropic value at room temperature.

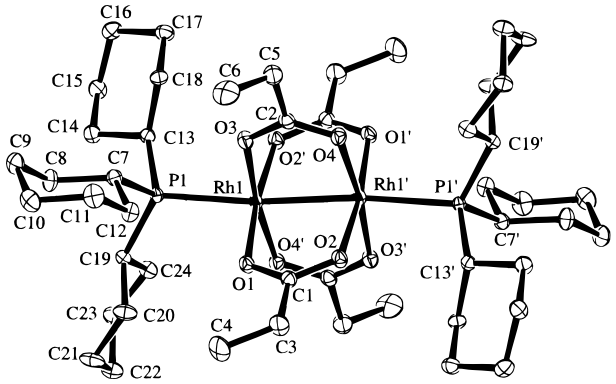

Figure 1. ORTEP drawing of $[Rh_2(O_2CEt)_4(Pcy_3)_2]^+$ in $[Rh_2(O_2CEt)_4(Pcy_3)_2]SbF_6 \cdot 2CH_2Cl_2$ (**5**·$2CH_2Cl_2$) showing the atomic numbering scheme. Vibrational ellipsoids are at the 50% level.

Table 3. Important Distances (Å) and Bond and Torsion Angles (deg) of the Cationic Radical in $[Rh_2(O_2CEt)_4(Pcy_3)_2]SbF_6 \cdot 2CH_2Cl_2$ (**5**·$2CH_2Cl_2$)

Bonded and Nonbonded Interatomic Distances			
Rh(1)−Rh(1′)	2.5086(4)	Rh(1)−O(3)	2.049(2)
Rh(1)−P(1)	2.3753(6)	Rh(1)−O(4′)	2.030(2)
Rh(1)−O(1)	2.035(2)	O(1)····O(2)	2.263(2)
Rh(1)−O(2′)	2.042(2)	O(3)····O(4)	2.263(2)
Bond Angles			
C(7)−P(1)−C(13)	108.0(1)	C(13)−P(1)−C(19)	104.8(1)
C(7)−P(1)−C(19)	107.9(1)		
Dihedral Angles			
O(1)−Rh(1)−Rh(1′)−O(2)		−1.85(7)	
O(3)−Rh(1)−Rh(1′)−O(4)		0.27(7)	

peak pairs at $E_{1/2}$ of −0.31 and −0.29 V vs Fc^+/Fc, respectively. These complexes were oxidized to their cationic radical salts by $FcSbF_6$ in CH_2Cl_2, and the resulting dark green salts were stable enough to be isolated in moderate yields. Frozen (77 K) CH_2Cl_2 solutions of these salts gave axially symmetric ESR spectra whose parallel and perpendicular features were 1:2:1 triplets arising from two equivalent ^{31}P nuclei. Their spin Hamiltonian parameters are listed in Table 2. The principal values of the g-tensors [g(parallel) ≅ 2.00 and g(perpendicular) > 2.00] indicate that the odd electron is accommodated in the σ_{RhRh} orbital.[4,8,11] The odd electron density on the phosphorus $3p_\sigma$ (σ with respect to the Rh−P axis) atomic orbital can be estimated from the anisotropy of the observed ^{31}P hyperfine coupling tensors by following the procedure reported previously[4b] as 0.20 and 0.19 for $\mathbf{1}^+$ and $\mathbf{2}^+$, respectively.

Structure of $[Rh_2(O_2CEt)_4(Pcy_3)_2]SbF_6 \cdot 2CH_2Cl_2$ (5·$2CH_2Cl_2$). The cationic radical and the SbF_6^- units are located on each of the two types of the crystallographic inversion centers. The anion is surrounded by hydrogen atoms of CH_2Cl_2 and of alkyl groups of axial and bridging ligands of the cationic radicals. Figure 1 shows an ORTEP view and the atom labeling scheme for the cationic radical. Table 3 summarizes important geometry parameters around the metal atoms.

Structure of $[Rh_2(O_2CEt)_4(PPr^i_3)_2]SbF_6$ (6). The crystal of this salt has two independent cationic units on inversion centers and an SbF_6 anion unit at a general position. The structures of the two independent cationic units resemble each other except for the configuration of the alkyl groups of the bridging ligands; an ORTEP view of only one unit is displayed in Figure 2. Pertinent bond lengths and angles are tabulated for both of the cationic units in Table 4.

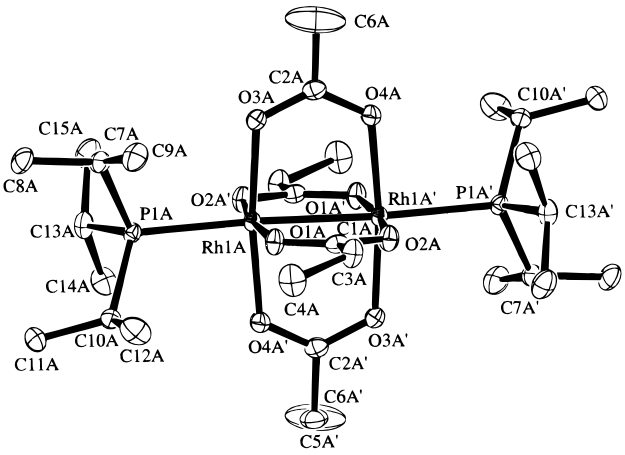

Figure 2. ORTEP drawing for one of two independent $[Rh_2(O_2CEt)_4(PPr^i_3)_2]^+$ units in $[Rh_2(O_2CEt)_4(PPr^i_3)_2]SbF_6$ (**6**) showing the atomic numbering scheme (with the suffix A). Replacement of the suffix A with B gives the numbering scheme for the other unit. Vibrational ellipsoids are at the 50% level.

Table 4. Important Distances (Å) and Bond and Torsion Angles (deg) in $[Rh_2(O_2CEt)_4(PPr^i_3)_2]SbF_6$ (**6**)

Bonded and Nonbonded Interatomic Distances			
Rh(1A)−Rh(1A′)	2.5105(4)	Rh(1B)−Rh(1B′)	2.5082(5)
Rh(1A)−P(1A)	2.3596(8)	Rh(1B)−P(1B)	2.3574(8)
Rh(1A)−O(1A)	2.033(2)	Rh(1B)−O(1B)	2.040(2)
Rh(1A)−O(2A′)	2.025(2)	Rh(1B)−O(2B′)	2.027(2)
Rh(1A)−O(3A)	2.035(2)	Rh(1B)−O(3B)	2.030(2)
Rh(1A)-O(4A′)	2.037(2)	Rh(1B)−O(4B′)	2.040(2)
O(1A)····O(2A)	2.254(3)	O(1B)····O(2B)	2.251(3)
O(3A)····O(4A)	2.261(3)	O(3B)····O(4B)	2.268(3)
Bond Angles			
C(7A)−P(1A)−C(10A)	113.6(1)	C(7B)−P(1B)−C(10B)	105.8(1)
C(7A)−P(1A)−C(13A)	104.8(1)	C(7B)-P(1B)-C(13B)	112.7(2)
C(10A)−P(1A)−C(13A)	104.9(1)	C(10B)-P(1B)-C(13B)	104.0(1)
Dihedral Angles			
O(1A)−Rh(1A)−Rh(1A′)−O(2A)		0.73(9)	
O(3A)−Rh(1A)−Rh(1A′)−O(4A)		0.02(9)	
O(1B)−Rh(1B)−Rh(1B′)−O(2B)		1.10(9)	
O(3B)−Rh(1B)−Rh(1B′)−O(4B)		0.74(9)	

Isolation and Structure of $[Rh_2(form)_4]ClO_4$ (7). Piraino and co-workers[21] synthesized **3**, showed that it can be oxidized to the corresponding stable cationic complex, and reported ESR data indicating the accommodation of its odd electron in the δ_{RhRh}^* orbital.[38] They isolated $[Rh_2(form)_4(H_2O)]CF_3CO_2$ formed by oxidation with AgO_2CCF_3 in $CHCl_3$ and reported its X-ray structure.[38] When oxidation of **3** was tried by using dry $AgClO_4$ in dry CH_2Cl_2, axial ligand-free cationic radical salt, **7**, was isolated. The geometry of **7** will be compared in the following section with that of **3** (axial ligand-free) to examine the geometry change arising from the ionization. The dimer unit of **7** lies on a 422 position in the space group *P*4/*nnc* and belongs to the D_{4h} point group. The ClO_4^- ion is located on the other 422 site and its arrangement is disordered to fit the symmetry of the site. Although Rh−Rh bonds and perchlorate ions are arranged alternatingly on a crystallographic 4-fold axis, the

(38) Bruno, G.; Schiavo, S. L.; Tresoldi, G.; Piraino, P. *Inorg. Chim. Acta* **1992**, *196*, 131.

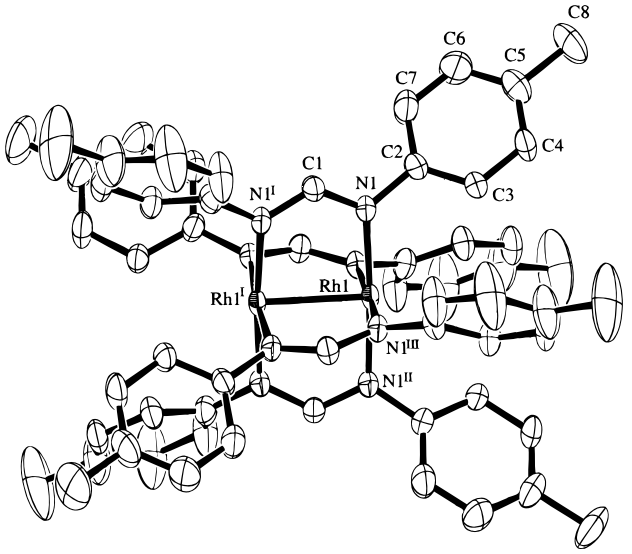

Figure 3. ORTEP view of $[Rh_2(form)_4]^+$ in $[Rh_2(form)_4]ClO_4$ (**7**) showing the atomic numbering scheme. Vibrational ellipsoids are at the 50% level.

Table 5. Important Distances (Å) and Torsion Angles (deg) in $[Rh_2(form)_4]ClO_4$ (**7**)

Bonded and Nonbonded Interatomic Distances			
Rh(1)−Rh(1^I)	2.447(1)	Rh(1)−N(1)	2.019(4)
N(1)····N(1^I)	2.331(6)		
Dihedral Angles			
N(1)−Rh(1)−Rh(1^I)−N(1^I)		−9.6(3)	

location of a Rh atom and its nearest O atoms of neighboring perchlorates is far from contacts. An ORTEP view of the cation is displayed in Figure 3. Table 5 summarizes important geometry parameters around the metal atoms.

Comparison of Geometry between Rh_2^{4+} and Rh_2^{5+} Complexes. Important geometrical parameters around the Rh_2 cores are summarized in Table 6 for all pairs of Rh_2^{4+} and Rh_2^{5+} complexes with common bridging and axial ligands known to us. The geometry differences of the bridging ligands between the neutral and the corresponding cationic complexes have not been detected beyond experimental errors as shown in the column of Eq····Eq in this table.

Geometrical changes due to the one-electron oxidation of **1** and **2** are most notable in Rh−Rh and Rh−P bond distances: the Rh−Rh lengths increased around 0.05 Å and the Rh−P decreased around 0.12 Å. The trend of the changes shows that the removal of an electron has taken place from the orbital of the Rh−Rh bonding and Rh−P antibonding character. The large changes in the Rh−P bond length are consistent with the ESR data which indicate that the σ_{RhRh} SOMO has a large density on the phosphorus atoms and with the prediction by Bursten and Cotton based on SCF Xα-SW calculations.[11] The pyramidality of the axial phosphine ligands was flattened upon the oxidation: the sums of the three C−P−C bond angles in the phosphine increased from 313.0(3)° to 320.7(3)° [$\Delta = +7.7$-(6)°] and from 313.0(6)° to 322.8(4)° [$\Delta = +9.8(10)°$; the average for the crystallographically independent dinuclear units A and B] for **1** and **2**, respectively. The sums of the corresponding three angles for tetrahedral and planar geometries are 328.4 and 360°, respectively, and their difference is 31.6°. The flattening of the phosphine pyramids observed for $\mathbf{1}^+$ and $\mathbf{2}^+$ is fairly large.

The change of the Rh−Rh bond length upon the σ_{RhRh} electron ionization of the $[Rh_2(O_2CEt)_4(PR_3)_2]$ complexes is smaller than that for the removal of a π_{RhRh}^* electron from $[Rh_2(OAc)_4(H_2O)_2]$ (0.07 Å).[19,39] This implies that the π_{RhRh}^* orbital in $[Rh_2(OAc)_4(H_2O)_2]$ is far more localized on the metal atoms than the σ_{RhRh} orbital in $[Rh_2(O_2CEt)_4(PR_3)_2]$.

Contrary to detectable effects of the ionization of a σ_{RhRh} or π_{RhRh}^* electron on the Rh−Rh bond length, the removal of a δ_{RhRh}^* electron results in small and nonsystematic changes of the Rh−Rh bond length (Table 6). The decrease of Rh−Eq distances upon the removal of a δ_{RhRh}^* electron exceeds those accompanying the removal of a σ_{RhRh}^* or π_{RhRh}^* electron. This would have originated from the π_{RhEq}^* character of the δ_{RhRh}^* orbital (namely, the delocalization of the δ_{RhRh}^* orbital onto the bridging ligands in the π antibonding phase).[5c] The δ_{RhRh}^* odd electron in $\mathbf{4}^+$, *cis*-(2,2)-$[Rh_2\{CH_3C(O)NH\}_4(H_2O)_2]^+$, **7**, and $[Rh_2(dpf)_4(CH_3CN)]^+$ is expected to be delocalized onto the π systems of their four bridging ligands forming a sterically interesting delocalized system.[18] The mixing of the δ_{MM}-type orbital with π orbitals of the bridging ligands has been pointed out by Granozzi and his colleagues[13] to explain the photoelectron spectra of $[Rh_2(form)_4]$, by Cotton and Feng[12] based on SCF-Xα calculations, by Lichtenberger and co-workers[40] on the basis of the incident photon energy dependence on the cross-section of the δ_{MoMo} ionization band in the PES of $[Mo_2(OAc)_4]$, and by Chisholm and co-workers based on the CV and the electronic spectrum of $[Mo_2(O_2CBu^t)_3(\mu_4\text{-}C_2O_4)Mo_2(O_2CBu^t)_3]$[41] and on the paramagnetic shifts in the ^1H NMR of $[Ru_2(O_2CR)_4]^{0/+}$.[42] The ionization of a δ_{RhRh}^* electron resulted in decrease of the Eq−Rh−Rh−Eq torsion angles when these angles are large in the neutral mother complexes {i.e., **3** and $[Rh_2(dpf)_4(CH_3CN)]$; dpf = $(PhN)_2CH$}.

DFT Calculations. Geometry was optimized for model complexes of **8**, **9**, **10**, and **11** and for low-lying doublet states of their cations by using the B3LYP DFT method. The calculated results in Table 7 have successfully reproduced the corresponding experimentally deduced ligand-dependent ground-state electron configurations of Rh_2^{5+} complexes. The calculated changes of the Rh−Rh and Rh−ligand bond lengths for the ground states of the model complexes are reasonably consistent with the corresponding experimental ones.

Comparison of geometry changes of low-lying doublet states for each of the model complexes shows that the σ_{RhRh} ionization induces enhanced shortening of Rh−Ax bonds (ca. −0.2 Å) due to σ_{RhAx}* character of the involved orbital ($^2A_1$ of $\mathbf{8}^+$ and $^2A_1$ of $\mathbf{9}^+$) and elongation of Rh−Rh bonds (ca. 0.06−0.15 Å; $^2A_1$ of $\mathbf{8}^+$, $^2A_1$ of $\mathbf{9}^+$, and $^2A_1$ of $\mathbf{11}^+$), where the rather small Rh−Rh bond length change for $\mathbf{8}^+$ is due to the decreased σ_{RhRh} character of the orbital. Among the calculated Rh−Eq bond length changes, enhanced decreases were obtained for the formation of δ_{RhRh}*-SOMO radicals (ca. −0.04 Å; $^2A_2$ of $\mathbf{8}^+$, $^2A_2$ of $\mathbf{9}^+$, ^2A_u of $\mathbf{10}^+$, and $^2A_2$ of $\mathbf{11}^+$). This arises from the delocalization of the δ_{RhRh}* orbitals onto the bridges in the π_{RhEq}* phase. Part of the enhanced Rh−Eq bond length shortening may have arisen from the increased Coulombic interaction between negatively charged Eq atoms and the Rh_2^{5+} core. The absolute values of the changes of Rh−Rh bond distances decreased depending on the symmetry of the ionizing orbital in the order of $\sigma_{RhRh} > \pi_{RhRh}^* > \delta_{RhRh}^*$ for each of the calculated low-lying doublet states of a cationic radical.

(39) Cotton, F. A.; DeBoer, B. G.; LaPrade, M. D.; Pipal, J. R.; Ucko, D. A. *Acta Crystallogr.* **1971**, *B27*, 1664.
(40) Lichtenberger, D. L.; Ray, C. D.; Stepniac, F.; Chen, Y.; Weaver, J. H. *J. Am. Chem. Soc.* **1992**, *114*, 10492.
(41) Cayton, R.; Chisholm, M. H. *J. Am. Chem. Soc.* **1989**, *111*, 8921.
(42) Chisholm, M. H.; Christou, G.; Folting, K.; Huffman, J. C.; James, C. A.; Samuels, J. A.; Wesemann, J. L.; Woodruff, W. H. *Inorg. Chem.* **1996**, *35*, 3643.

Table 6. Geometry Difference (Å, deg) between Lantern-Type Rh_2^{4+} and Rh_2^{5+} Complexes

Eq and Ax ligands	oxdtn state[a]	Rh−Rh[b]	Rh−Eq[b,c]	Rh−Ax[b,c]	torsn[b,c,d]	Eq···Eq[b,c,e]	SOMO[f]
$(EtCO_2)_4$	Rh_2^{5+} [g]	2.5086(4)	2.039(10)	2.3753(6)	1.1(8)	2.263(2)	σ_{RhRh}
$(Pcy_3)_2$	Rh_2^{4+} [h]	2.4618(4)	2.048(10)	2.4868(6)	1.0(7)	2.255(2)	
	Δ	+0.0468(8)	−0.009(20)	−0.112(1)	+0.1(15)	+0.008(4)	
$(EtCO_2)_4$	Rh_2^{5+} [i]	2.5094(12)	2.033(8)	2.3585(11)	0.6(6)	2.259(9)	σ_{RhRh}
$(PPr^i_3)_2$	Rh_2^{4+} [j]	2.4601(5)	2.048(4)	2.4978(8)	0.9(5)	2.247(4)	
	Δ	+0.049(2)	−0.015(12)	−0.139(2)	−0.3(11)	+0.012(13)	
$(CH_3CO_2)_4$	Rh_2^{5+} [k]	2.3165(20)	2.014(15)	2.22(2)	0.6(4)	2.24(2)	π_{RhRh}*
$(H_2O)_2$	Rh_2^{4+} [l]	2.3855(5)	2.039(8)	2.310(3)	0.9(4)	2.248(4)	
	Δ	−0.069(3)	−0.025(23)	−0.09(2)	−0.3(8)	−0.01(2)	
$(mhp)_4$	Rh_2^{5+} [m]	2.3591(7)	2.026(3)/1.978(8)[n]		3.1(4)	2.307(4)	δ_{RhRh}*
none	Rh_2^{4+} [o]	2.3682(5)	2.043(4)/2.014(12)[n]		3.6(7)	2.310(5)	
	Δ	−0.0091(12)	−0.017(7)/−0.036(20)[n]		−0.5(11)	−0.003(9)	
$[CH_3C(O)NH]_4$	Rh_2^{5+} [p]	2.399(1)	1.976(3)/2.030(5)[n]	2.281(2)	1.4(9)	2.259(4)	δ_{RhRh}*
$(H_2O)_2$	Rh_2^{4+} [q]	2.415(1)	2.008(8)/2.073(4)[n]	2.352(2)	0.6(4)	2.269(4)	
	Δ	−0.016(2)	−0.032(11)/−0.043(9)[n]	−0.071(4)	+0.8(13)	−0.010(10)	
$(form)_4$	Rh_2^{5+} [r]	2.447(1)	2.019(4)		9.6(3)	2.331(6)	δ_{RhRh}*
none	Rh_2^{4+} [s]	2.4336(4)	2.050(5)		16.7(2)	2.348(8)	
	Δ	+0.013(1)	−0.031(9)		−7.1(5)	−0.017(14)	
$(dpf)_4$ [t]	Rh_2^{5+} [u]	2.466(1)	2.035(4)/2.025(4)[v]	2.074(6)	12.5(3)	2.321(9)	δ_{RhRh}*
CH_3CN	Rh_2^{4+} [w]	2.459(1)	2.062(2)/2.066(2)[v]	2.106(4)	16.8(2)	2.310(4)	
	Δ	+0.007(2)	−0.027(6)/−0.041(6)[v]	−0.032(10)	−4.3(5)	+0.011(13)	

[a] $\Delta = x(Rh_2^{5+}) - x(Rh_2^{4+})$. [b] Average value. [c] Eq and Ax denote ligating atom of equatorial bridging and axial ligands, respectively. [d] Eq−Rh−Rh−Eq torsion angle. [e] Nonbonded distance between the two ligation atoms in a bridging ligand. [f] SOMO of Rh_2^{5+} complex assigned by ESR. [g] $[Rh_2(O_2CEt)_4(Pcy_3)_2]SbF_6 \cdot 2CH_2Cl_2$ (**5**·$2CH_2Cl_2$) at −147 °C, present work. [h] $[Rh_2(O_2CEt)_4(Pcy_3)_2]$ (**1**) at −147 °C, present work. [i] $[Rh_2(O_2CEt)_4(PPr^i_3)_2]SbF_6$ (**6**) at −144 °C, present work. [j] $[Rh_2(O_2CEt)_4(PPr^i_3)_2]$ (**2**) at −62 °C, present work. [k] $[Rh_2(O_2CCH_3)_4(H_2O)_2]ClO_4 \cdot H_2O$.[16] [l] $[Rh_2(O_2CCH_3)_4(H_2O)_2]$ at 21 °C.[39] [m] $[Rh_2(mhp)_4]SbCl_6 \cdot CH_2ClCH_2Cl$ at −150 °C.[18] [n] r(Rh−N)/r(Rh−O). [o] $[Rh_2(mhp)_4] \cdot CH_2Cl_2$ (**4**·CH_2Cl_2) at −135 °C, present work. [p] $[Rh_2\{CH_3C(O)NH\}_4(H_2O)_2]ClO_4$.[16] [q] $[Rh_2\{CH_3C(O)NH\}_4(H_2O)_2] \cdot 3H_2O$ at 21 °C.[36] [r] $[Rh_2(form)_4]ClO_4$ at −20 °C, present work. [s] $[Rh_2(form)_4]$ at room temperature.[21] [t] dpf = $(C_6H_5N)_2CH$. [u] $[Rh_2(dpf)_4(CH_3CN)]ClO_4$.[17] [v] Two nonequivalent Rh−N_{Eq} bonds. [w] $[Rh_2(dpf)_4(CH_3CN)]$.[17]

Table 7. Optimized Geometries and Relative Energies of Rh_2^{4+} and Rh_2^{5+} Complexes[a]

state	SOMO	rel E[b]	Rh−Rh/Å[c]	Rh−Eq/Å[c,d]	Rh-Ax/Å[c,d]
		$[Rh_2(O_2CH)_4(PH_3)_2]^{0/+}$ (**8**$^{0/+}$) in C_{2v}			
Rh_2^{5+} $^2A_1$	σ_{RhRh}, σ_{RhP}*	0.0	(0.0674)	(−0.011)	(−0.194)
Rh_2^{5+} $^2A_2$	δ_{RhRh}*	9.0	(0.0056)	(−0.039)	(0.0273)
Rh_2^{5+} $^2B_2$	π_{RhRh}*	13.0	(−0.0261)	(−0.02)	(0.0531)
Rh_2^{5+} $^2B_1$	π_{RhRh}	26.4	(0.1099)	(−0.02)	(0.0099)
Rh_2^{4+} $^1A_1$		−170.8	2.4983	2.093	2.5490
		$[Rh_2(O_2CH)_4(OH_2)_2]^{0/+}$ (**9**$^{0/+}$) in C_{2v}			
Rh_2^{5+} $^2B_1$	π_{RhRh}*	0.0[e]	(−0.0442)	(−0.026)	(−0.0812)
Rh_2^{5+} $^2A_2$	δ_{RhRh}*	1.4	(−0.0054)	(−0.042)	(−0.0436)
Rh_2^{5+} $^2B_2$	π_{RhRh}*	4.4	(−0.0443)	(−0.028)	(−0.0453)
Rh_2^{5+} $^2A_1$	σ_{RhRh}	21.8	(0.1072)	(−0.013)	(−0.1865)
Rh_2^{4+} $^1A_1$		−173.3	2.4570	2.090	2.2670
		cis-(2,2)-$[Rh_2(HNCHO)_4(OH_2)_2]^{0/+}$ (**10**$^{0/+}$) in C_i			
Rh_2^{5+} ^2A_u	δ_{RhRh}*	0.0	(−0.0092)	(−0.030/−0.052)[f]	(−0.0478)
Rh_2^{5+} ^2A_g	π_{RhRh}*	14.8	(−0.0587)	(0.005/−0.04)[f]	(−0.1018)
Rh_2^{4+} ^1A_g		−156.9	2.4749	2.049/2.117[f]	2.3431
		$[Rh_2(HNCHNH)_4]^{0/+}$ (**11**$^{0/+}$) in C_{2v}			
Rh_2^{5+} $^2A_2$	δ_{RhRh}*	0.0	(−0.0224)	(−0.0346)	
Rh_2^{5+} $^2B_1$	π_{RhRh}*	35.8	(−0.0722)	(−0.005)	
Rh_2^{5+} $^2A_1$	σ_{RhRh}	74.3	(0.1251)	(−0.0055)	
Rh_2^{4+} $^1A_1$		−120.2	2.4965	2.0772	

[a] Geometries of the Rh_2^{5+} complexes were optimized for each of low-lying doublet states. [b] Energies relative to the lowest doublet state of the Rh_2^{5+} complex in kcal/mol. [c] Bond lengths for the Rh_2^{4+} complexes and bond length changes in parentheses arising from one-electron oxidation for the Rh_2^{5+} complexes in Å. [d] Average. [e] At the $^2B_1$ optimized geometry, the energies of the $^2A_2$ and $^2B_2$ states were calculated to be 2.7 and 6.1 kcal/mol higher than the energy for the $^2B_1$ state, respectively. [f] Rh−N_{eq}/Rh−O_{eq}.

The sum of the three H−P−H bond angles around a phosphorus atom of **8** was calculated to increase from 291.0° to 310.0° ($\Delta = +18.9°$) upon the σ_{RhRh} ionization. This increase is parallel to the observation of $\Delta = +7.7(6)°$ and $\Delta = +9.8(10)°$ for **6** and **7**. The electron occupancy and hybridization of the phosphine lone-pair orbital in **8** and the $^2A_1$ state (the σ_{RhRh} radical state) of **8**$^+$ are analyzed by the NBO method for the Lewis structures of $[Rh_2^{4+}][HCO_2^-]_4[PH_3]_2$ and $[Rh_2^{5+}][HCO_2^-]_4[PH_3]_2$, respectively. The NBO electron occupancy on the phosphine lone-pair orbital decreased from 1.726 for **8** to 1.326 for **8**$^+$. The flattening of the phosphine pyramid of **8**$^+$ can be interpreted as to arise from this decrease by following the valence-shell electron pair repulsion theory scheme. The NBO hybridization of the phosphine lone-pair orbital of **8** was calculated as $sp^{3.02}$ whereas that of **8**$^+$ as $sp^{4.93}$. The average NBO hybridization of the PH bonds was $sp^{2.95}$ for **8** and $sp^{2.57}$ for **8**$^+$. The flattening of the phosphine pyramid of **8**$^+$ can also be explained as to be induced to shift the phosphorus 3s component to the PH bonds from the lone-pair orbital involved in the ionization (Bent rule[43]). The force constants for the Rh−P bond length of **8** and the $^2A_1$ state of **8**$^+$ were calculated to be 0.067 and 0.164 hartree/Å^2, respectively. This result shows also

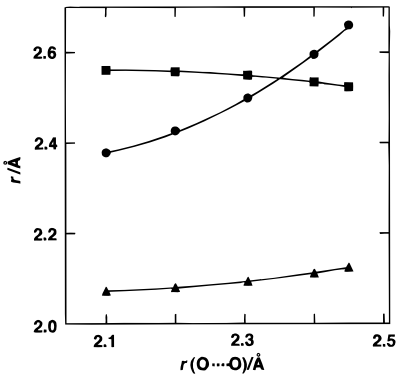

Figure 4. Calculated dependence of optimized Rh−Rh (dots), Rh−P (squares) and Rh−O (triangles) bond distances on the O····O nonbonded distance of the bridging formates of $[Rh_2(O_2CH)_4(PH_3)_2]$. The O····O distance was artificially varied by changing the O−C−O bond angles.

that the Rh−P bond is strengthened upon the removal of an electron from the orbital with σ_{RhP}* character when **8** is ionized.

The observed fairly large decrease (0.071 Å) of the Rh−Ax bond length induced by the removal of a δ_{RhRh}* electron from *cis*-(2,2)-$[Rh_2\{CH_3C(O)NH\}_4(H_2O)_2]$[16,36] was also reproduced by the DFT calculation as the 0.048 Å difference in the $\mathbf{11}^{0/+}$ pair. The δ_{RhRh}* orbital is symmetry-forbidden to delocalize onto the axial ligands. The force constant estimated for the $Rh-O_{ax}$ bond length was 0.078 hartree/Å^2; this is small when compared with that for the $Rh-O_{eq}$ bond (0.17 hartree/Å^2). The force constant of the $Rh-O_{ax}$ bond length for $\mathbf{11}^+$ was calculated as 0.089 hartree/Å^2. The natural atomic charges of the axial O and the Rh atoms were calculated as −0.935 e and +0.790 e, respectively for **11** and as −0.954 e and +0.915 e, respectively for $\mathbf{11}^+$. We suppose that the large decrease of the $Rh-O_{ax}$ bond distance upon the one-electron oxidation of **11** originates from the smallness of the force constants for this bond and from the increased Coulombic interaction between the more positively charged metal atom and the lone pair on the axial ligand in $\mathbf{11}^+$.

To see the dependence of the geometry around the Rh atoms on the Eq····Eq nonbonded distance of a bridging ligand, we examined the dependence of the optimized lengths of Rh−Rh, Rh−P, and Rh−O bonds on the O····O distance of **8** by artificially varying the O−C−O bond angle of the bridges (Figure 4). The calculated Rh−Rh bond length heavily depends on the O····O nonbonded distance with an incline of nearly 0.8, showing the Rh−Rh length is held rather rigidly by the four bridges. This can be an origin of the experimentally observed rather retarded dependence of the Rh−Rh bond length of the present $[Rh_2(bridge)_4L_2]^{0/+}$ complexes on the electron configuration. If some of the bridging ligands were substituted by nonbridging ones, the metal−metal bond length change is expected to be larger. The Rh−P and Rh−O bond lengths show minor dependence on the O····O separation and are expected to change more sensitively.

The calculated Mulliken and natural atomic spin populations are summarized in Table 8. The spin population in the $\mathbf{8}^+$ σ_{RhRh} radical was most extensively delocalized onto the ligands among the calculated radicals and it was almost exclusively onto the axial phosphine ligands. The atomic spin population on the axial phosphine ligand exceeded that on the rhodium atom. This trend has been also observed in the Hartree−Fock[8] and the SCF Xα-SW calculations.[11] The spin population in $\mathbf{10}^+$ and $\mathbf{11}^+$ δ_{RhRh}* radicals is moderately delocalized onto the bridging ligands, and that in the $\mathbf{9}^+$ π_{RhRh}* radical is rather localized on the rhodium atoms. These characteristics of spin distribution may be helpful for design of materials with electric conductance or magnetism by utilizing these lantern-type complexes.

Table 8. Mulliken and Natural (in Parentheses) Atomic Spin Populations Calculated for Rh_2^{5+} Complexes

complex and SOMO	ρ(Rh)	ρ(bridge)[a]	ρ(axial)[b]
$[Rh_2(O_2CH)_4(PH_3)_2]^+$	0.218	−0.005	0.293
σ_{RhRh}, σ_{RhP}*	(0.188)	(0.0002)	(0.312)
$[Rh_2(O_2CH)_4(H_2O)_2]^+$	0.434[c]	0.028[c]	0.009[c]
π_{RhRh}*	(0.426)	(0.031)	(0.012)
$[Rh_2(HNCHNH)_4]^+$	0.260	0.120	
δ_{RhRh}*	(0.255)	(0.122)	
$[Rh_2(HNCHO)_4(H_2O)_2]^+$	0.312	0.095	−0.001
δ_{RhRh}*	(0.299)	(0.101)	(−0.001)

[a] Average for the sum of the atomic spin populations over all the atoms of a bridging ligand. [b] The sum of the atomic spin populations over all the atoms of an axial ligand. [c] The average of the spin populations for each of the degenerate pair of π_{RhRh}* odd-electron orbital states, i.e., the average over $^2B_1$ and $^2B_2$ states at the optimized geometry for the $^2B_1$ state.

Concluding Remarks

(1) The σ_{RhRh} orbital in $[Rh(O_2CR)_4(PR_3)_2]$ is extensively mixed with the axial phosphine lone-pair orbitals, and the removal of an electron from this orbital results in the elongation of the Rh−P bond (0.112−0.139 Å) and the flattening of the phosphine pyramid. (2) The δ_{RhRh}* orbital is moderately delocalized onto the π system of the bridging ligands, and the removal of an electron from this orbital induces 0.017−0.041 Å shortening of Rh−Eq bonds. (3) Unrestricted DFT calculations with the B3LYP potential functional reproduce the ligand dependence of the electron configuration of the Rh_2^{5+} complexes. (4) Geometry optimization with the DFT method reasonably reproduces the geometry changes induced by one electron oxidation of Rh_2^{4+} complexes.

Acknowledgment. We are grateful for the financial support from the Ministry of Education, Science and Culture of Japan. The DFT calculations were performed on the IBM SP2 workstation cluster at the computer center of the Institute for Molecular Science (Okazaki).

Supporting Information Available: ORTEP views of **1**, **2**, and **4**·CH_2Cl_2, tables of position and thermal parameters, bond lengths and bond and dihedral angles of **1**, **2**, **4**·CH_2Cl_2, **5**·$2CH_2Cl_2$, **6**, and **7** and of Cartesian coordinates of the geometry-optimized model complexes, and potential curves to estimate the force constants of Rh−O and Rh−P bonds in $\mathbf{8}^{0/+}$ and of Rh−O bonds in $\mathbf{11}^{0/+}$(53 pages, print/PDF). See any current masthead page for ordering information and Web access instructions.

JA9712940

(43) Bent, H. A. *Chem. Rev.* **1961**, *61*, 275.